Jun 25th, 12:00 AM - Jun 27th, 12:00 AM

Large-Eddy Simulations of T-shaped Open-Channel Confluences With Different Downstream Channel Widths

Pedro Xavier Ramos
Ghent University, pedro.ramos@ugent.be

Laurent Schindfessel
Ghent University

João Pedro Pêgo
University of Porto

Tom De Mulder
Ghent University

7th International Junior Researcher and Engineer Workshop on Hydraulic Structures, IJREWHS'19, B. HEINER and B. TULLIS (Eds), Report 3, U.S. Bureau of Reclamation, Denver, CO, USA - ISBN 978-0-578-69809-0
https://doi.org/10.26077/z99p-xs05

Large-Eddy Simulations of T-shaped open-channel confluences with different downstream channel widths

Pedro Xavier RAMOS
Hydraulics Laboratory, Department of Civil Engineering, Ghent University, Sint-Pietersnieuwstraat 41 B5, Ghent B-9000, Belgium, Email: Pedro.Ramos@UGent.be.
Laurent SCHINDFESSEL
Hydraulics Laboratory, Department of Civil Engineering, Ghent University, Sint-Pietersnieuwstraat 41 B5, Ghent B-9000, Belgium.
João Pedro PÊGO
Faculty of Engineering – University of Porto, Rua do Dr. Roberto Frias, 4200-465 Porto, Portugal.
Tom De MULDER
Hydraulics Laboratory, Department of Civil Engineering, Ghent University, Sint-Pietersnieuwstraat 41 B5, Ghent B-9000, Belgium.

Abstract: Confluences of open-channel flows are common in nature as well as in urban drainage networks and in hydraulic structures. The complex hydrodynamics is often studied in schematized, right-angled confluences. In this paper, the influence of the downstream channel width onto time-averaged and turbulent flow features will be investigated numerically, based on Large-Eddy Simulations. For one flow situation, i.e. flow ratio and downstream Froude number, two geometries will be compared: a discordant width case, which was studied experimentally by Yuan et al. (2016) in a flume with a wider downstream channel than the upstream mean and tributary channels, and the corresponding concordant width case, in which the downstream channel has the same width as the confluent channels. The widening of the downstream channel turns out to reduce the backwater effects, the flow contraction and the associated water surface depression. Moreover, the three-dimensionality of the recirculation zone in the mean flow is enhanced due to complex flow patterns, resulting in a reduced width and length of the recirculation zone in the lowest third of the water column. Finally, the respective cores of high values of the dimensionless TKE and Reynolds shear stress, that persist over the water column, have lower peak values in the discordant width case and the shape of those cores is more distorted, especially near the bed.

Keywords: *open-channel confluence; unequal widths; Large-Eddy Simulation; CFD.*

INTRODUCTION

Confluences of open-channel flows are ubiquitous features in fluvial networks, urban drainage networks and even in hydraulic structures (e.g. outfalls, fish passes). Confluences are important

locations in those networks as they regulate the water levels, the mixing phenomena of the incoming flows and the transport and deposition of sediments, pollutants and nutrients (Best, 1987; Biron et al. 1996; Boyer et al. 2006; Rice et al., 2008; De Serres et al. 1999; Ludeña et al. 2017; Cushman-Roisin and Constantinescu, 2019).

The flow features in the confluence hydrodynamics zone (CHZ) are complex and are often studied in schematized geometries consisting of straight branches and sharp junction corners. Best (1987) developed a conceptual model discerning the features indicated (in planform) in Figure 1: a flow stagnation zone, a flow deflection zone, a flow recirculation zone (RZ), a zone of maximum velocity, a gradual flow recovery area and shear layers. The characteristics of these (three-dimensional) flow features depend, among other factors, upon the confluence angle between the inflowing branches, the ratio of the inflowing momentum fluxes, the tailwater Froude number and the bed elevation discordance (e.g. Đorđević, 2013; Biron et al. 1996; Penna et al. 2018; Birjukova-Canelas et al. 2019).

Among the schematized geometries, the right-angled confluences of a main channel and a tributary channel have been investigated the most extensively. The experimental data of Weber et al. (2001) pertain to lab experiments in such a T-shaped confluence with horizontal and concordant beds (i.e. no bed elevation discordance is present between the main and the tributary channels) and concordant widths (i.e. the post-confluence channel has the same width as the incoming channels). These data have been used frequently for validation of numerical models. By means of validated numerical models, the mean (i.e. time-averaged) and turbulent flow features in the CHZ can then be studied in more detail in similar or variant geometries and flow conditions as were studied experimentally (e.g. Huang et al., 2002; Constantinescu et al. 2001; Yang et al., 2013; Schindfessel et al., 2015; Ramos et al., 2019a,b).

For many years, the study of Weber et al. (2001) was one of the few studies investigating experimentally the flow structure of a T-shaped open-channel confluence. More recently, Yuan et al. (2016) experimentally studied a right-angled open-channel confluence with a wider post-confluence channel and adopting a higher time-resolution of the velocity measurements.

The present paper wants to contribute to assessing the effects of width discordance between the confluent channels on the confluence flow features. To this end, a numerical model based upon Large-Eddy Simulations will be first set up and validated for one of the flow cases investigated experimentally by Yuan et al. (2016) in the confluence with a wider downstream channel, which will be further referred to as the discordant width case. Then, the model will be adapted to simulate the corresponding concordant width case (i.e. the downstream channel will be narrowed to have the same width as the upstream channels).

The effect of width discordance onto the water surface elevations, the three-dimensional

structure of the recirculation zone and some turbulent flow features will then be assessed.

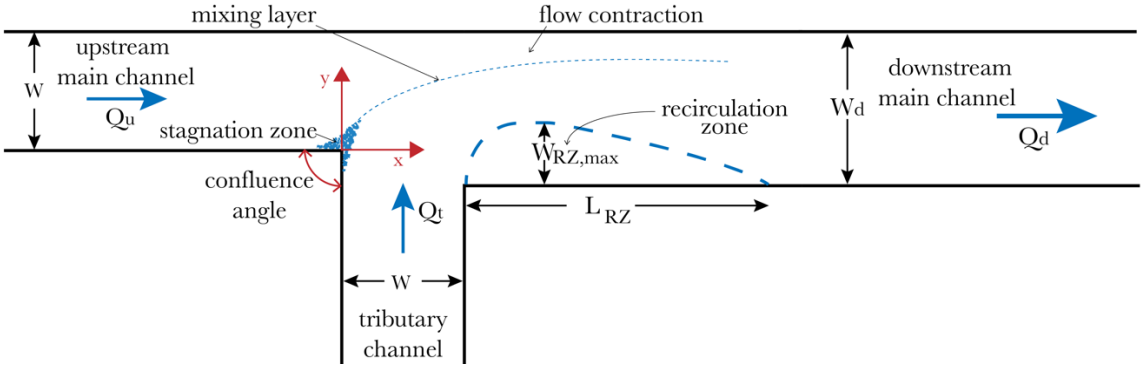

Figure 1. Schematic plan-view of the flow features in a right-angled open-channel confluence with channels of equal width (after Best, 1987) with coordinate system, nomenclature and recirculation zone dimensions at a given elevation z above the bed.

HYDRAULIC CONDITIONS

In this work, a right-angled confluence of open channels with a rectangular cross-section and with horizontal and concordant beds is considered. Let W be the width of the main upstream channel and the tributary channel and W_d the width of the downstream (i.e. post-confluence) channel (Figure 1). Two cases will be studied, having a different width discordance ratio:

$$\omega = {W}/{W_d} \quad (1)$$

The discordant width case (ω=0.75) has a wider downstream channel than the upstream channels (Figure 1) and corresponds to the lab experiment with fixed, horizontal and concordant beds by Yuan et al. (2016), which is referred to in the latter paper as "case two". The associated hydraulic conditions are given in Table 1, in which the discharge ratio is defined as follows:

$$q = {Q_u}/{Q_d} = {Q_u}/{(Q_u + Q_t)} \quad (2)$$

where Q_u and Q_t are the incoming discharge of the main channel and the tributary, respectively, and Q_d is the downstream discharge. The downstream Froude number is given by:

$$Fr_d = {U_d}/{\sqrt{g h_d}} \quad (3)$$

where $U_d=Q_d/(h_d W_d)$ is the cross-sectionally averaged downstream velocity, h_d the downstream flow depth and g the gravitational acceleration.

Table 1. Flow case with discordant width (ω=0.75) experimentally investigated by Yuan et al. (2016)

Q_u [l/s]	**Q_t [l/s]**	**Q_d [l/s]**	**q [-]**	**W** [m]	**W_d** [m]	**ω [-]**	**h_d** [m]	**U_d [m/s]**	**Fr_d [-]**
3.9	6.0	9.9	0.40	0.30	0.40	0.75	0.163	0.152	0.12

The concordant width case (ω=1.00) has a downstream channel width which is identical to the width of the upstream channels. Note that the concordant width case has not been investigated experimentally by Yuan et al. (2016). It will be simulated at the same hydraulic conditions (q, Fr_d) as the discordant width case (ω=0.75). As a consequence, the downstream water depth and cross-sectionally averaged velocity in the concordant width case (Table 2) differ from the discordant width case values (Table 1). Note that for both the discordant and the concordant width case, the origin of the coordinate system (Figure 1) is at the upstream confluence corner (x=0, y=0) and at bed elevation (z=0).

Table 2. Flow case with concordant width (ω=1.00)

Q_u	Q_t	Q_d	q	W	W_d	ω	h_d	U_d	Fr_d
[l/s]	**[l/s]**	**[l/s]**	**[-]**	[m]	[m]	**[-]**	[m]	**[m/s]**	**[-]**
3.9	6.0	9.9	0.40	0.30	0.30	1.00	0.197	0.167	0.12

NUMERICAL METHODOLOGY

Large-Eddy Simulations within the OpenFOAM toolbox

The numerical simulations in the present contribution are conducted within the three-dimensional computational fluid dynamics (CFD) software OpenFOAM, version 5.0. A Large-Eddy Simulation approach is adopted, requiring to solve the spatially-averaged continuity and Navier-Stokes equations, governing an unsteady, incompressible and viscous flow. As a Subgrid Scale Model (SGS), the standard Smagorinsky model is used, with a constant C_s of 0.158. In the OpenFOAM toolbox, the governing equations are discretized using the Finite Volume Method (FVM). The selected discretization schemes are second order accurate in time and space. The discretized equations are coupled and solved using the PISO algorithm.

Boundary conditions

In the present work, a rigid-lid approach is adopted as free surface treatment. This implies that the free surface is replaced by a frictionless and impermeable upper boundary of the computational domain. Ramos et al. (2019a) indicates that the implementation of a flat rigid-lid within the simulation of an open-channel confluence might not be valid close to the contracted section (i.e. adjacent to the recirculation zone) because the flow undergoes an acceleration that causes the water surface to drop substantially. With that in consideration, the present LES (Large-Eddy simulations) are run with a curved rigid-lid, approximating the numerical mesh height to the real flow depth. This curved rigid-lid will be defined by simulating first a flat rigid-lid (at an elevation z_{lid} above the bed) case and then converting the predicted time-averaged pressure field (P) onto the lid into an elevation of a virtual free surface (h), according to Equation (4):

$$h\,(x,y) = z_{lid} + \frac{P(x,y,z_{lid})}{\rho g} \quad (4)$$

Note that the latter equation implicitly assumes the hydrostatic pressure law to hold. On both the flat and the curved rigid-lids, zero shear stress and zero normal velocity conditions are imposed on the lids. The foregoing approach is further explained in Ramos et al. (2019a). In the present study, the low downstream Froude number of Fr_d = 0.12 (Table 1 and Table 2) suggests that the water surface variations are less pronounced as compared to the confluence flow cases studied in Ramos et al. (2019a), in which Fr_d, was 0.37. Nevertheless, the abovementioned methodology will be applied in this paper and only results of curved rigid-lid simulations will be shown.

For each of the two cases, ω=0.75 and ω=1.00, an impression of the adopted curved rigid-lid shape is given in Figure 2, by means of three longitudinal transects along the main and downstream channel.

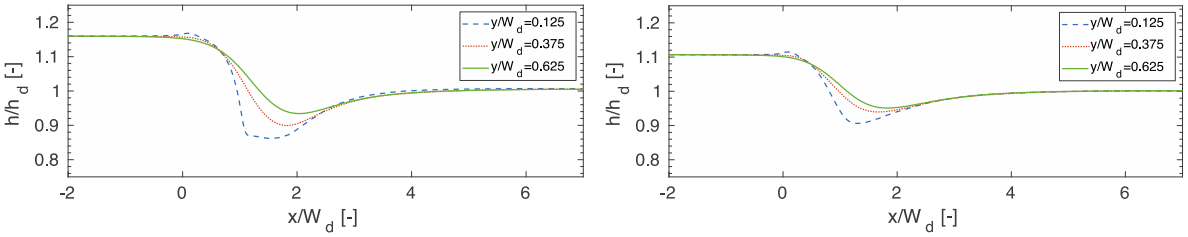

Figure 2. Curved rigid-lid shape indicated by three longitudinal transects along main and downstream channel (left: ω=1.00, right: ω=0.75).

In the present LES simulations, the wall boundary layers will not be fully resolved, with wall functions being adopted instead (see also Schindfessel *et al.*, 2015). This approach requires the first node to be located at $z^+ \approx 30-300$ (Rodi, Constantinescu and Stoesser, 2013; Schindfessel, 2017).

Since a LES resolves a relatively big part of the turbulence and to approach the model to reality, the inlet velocity should also be turbulent and fully developed. In the present numerical set up, this is achieved by means of a so-called precursor simulation, which basically means that a periodic channel is simulated and its turbulent velocity is used as an inlet condition.

For the pressure variable, a zero value is imposed at the outlet and a zero gradient at the inlets (x/W_d=-5; y/W_d=-5), the walls and the rigid-lid. For the subgrid-scale viscosity a zero gradient is imposed everywhere, except at the walls, where the aforementioned wall model is implemented.

Mesh

A block-structured mesh has been defined for the present numerical investigation (Table 3) after a mesh sensitivity analysis of the results. Grading of the cell size is adopted, yielding a higher resolution in the confluence zone and a smooth transition between the different blocks. The mesh for a flat rigid-lid simulation is deformed for the subsequent curved rigid-lid

simulation, based upon the methodology suggested by Rameshwaran and Naden (2004), and adopted and described in Ramos et al. (2019a): along each vertical grid line (i.e. the z direction), the highest grid point is shifted to coincide with the curved surface defined by Equation (4), whereas the near-wall point is kept in place in order to maintain the dimensionless wall-normal distance, z^+, constant and apply the wall function always under the same circumstances. The grid points in between are gradually redistributed along the vertical gridline (see Figure 4 in Ramos et al., 2019a). Our mesh sensitivity analysis shows that a coarser resolution than adopted in this paper will miss the secondary currents, like it is reported for another open-channel confluence in Ramos et al. (2019a) and in open-channel flows in general by Talebpour and Liu (2019). Therefore, special care was devoted to the mesh independence in terms of secondary flow results.

Table 3. Number of mesh cells for each simulation.

Case	upstream channels	main and tributary		downstream channel			total
	longitudinal (length=5W)	lateral (W=0.30 m)	vertical (h_d=0.18 W)	longitudinal (length=8 W)	lateral (W=0.40 m)	vertical (h_d=0.18 W)	number of cells
ω=0.75	600	100	45	850	120	25	4.2×10^6
ω=1.00					90		3.7×10^6

Model verification

The mesh used in the present paper (Section 3.4) is defined on the basis of a mesh sensitivity and independency analysis, as well as on the validation described in Section 4. Like it was already stated, as a consequence of the use of wall functions, the wall-normal distance of the first grid cells along the sidewalls and the bed should meet the criterion $30<z^+<300$. This condition is met for all the simulations, with z^+ being usually above 30, except for the zones of low flow velocity. These minor exceptions are expected and accepted, especially in the stagnation zone (McSherry et al., 2013; Schindfessel et al., 2015). To obtain the LES results presented in this paper, the simulations have advanced more than 600 seconds, before the data collection started. This initialization time corresponds to 33T (where $T=12W/U_d$ is an approximate flow-through time for the 12W long main channel). Data collection and time-averaging span an additional 75T of simulation (1350 s).

Computational resources

The simulations were computed on a 2×16-core Intel E5-2670 (Sandy Bridge @ 2.6 GHz). The total computational cost of the simulation is approximately 4200 CPU hours. Since the numerical domain is decomposed in 36 sub-domains, the real computational time, due to the parallel processing capabilities, is of 116 hours for each simulation.

RESULTS

Validation of the simulations

Figure 3 depicts the time-averaged horizontal velocity fields near the free surface (red arrows) and near the bed (black arrows) as predicted by the present simulation with discordant widths and as measured by Yuan et al. (2016) in the laboratory. The discrepancies, especially regarding the near bed flow (black arrows), between the LES results and the experiments suggest that the RZ is wider in the simulations. The simulated and measured velocities have the same order of magnitude and, despite the aforementioned discrepancies, the agreement is satisfactory.

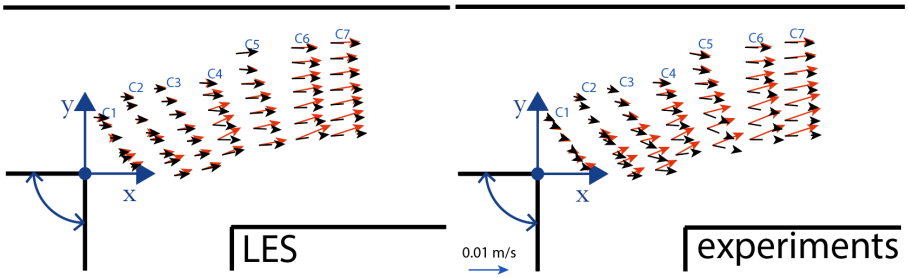

Figure 3. Horizontal velocity fields in the discordant width case (ω=0.75), close to the bed (z/h_d=0.12; black arrows) and close to the free surface (z/h_d=0.8; red arrows), as predicted by the LES simulation (left) and measured by Yuan et al. 2016 (right).

The turbulent kinetic energy (TKE) is shown in Figure 4 for the experiments and in the simulations of the case with ω=0.75. The vertical profiles are located in the cross-sections (C2, C3 and C5) depicted in Figure 3, more specifically in the location where the measured TKE assumes its maximum value in the experimental data of (Yuan et al. 2016). Note that in Figure 3, the vertical coordinate z is non-dimensionalized with respect to the local water depth, h'. The agreement is fair.

Figure 4.b shows the vertical profiles of the measured and simulated Reynolds shear stress ($\overline{u'v'}$) in the same locations as in Figure 4.a. Typically, the higher values occur at about half-depth, both in the experiments and in the simulations. Again, the results suggest a fairly confident validation of the simulations.

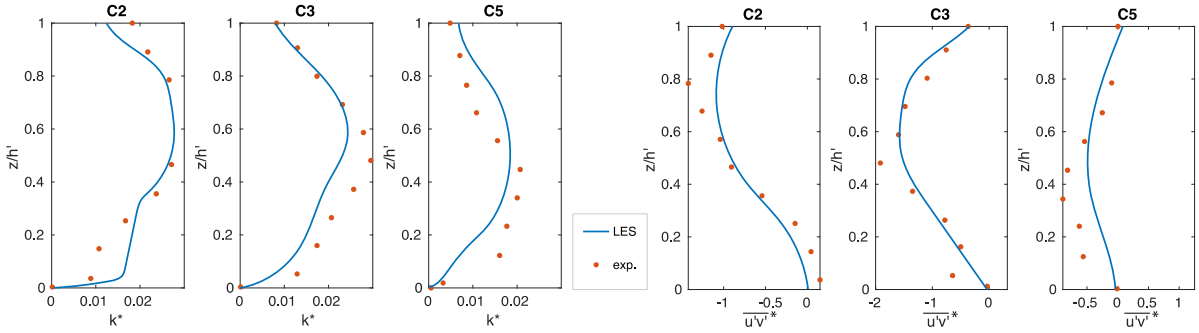

Figure 4. a. (left) Vertical profiles of dimensionless TKE ($k^*=TKE/U_d^2$) in the core of the mixing layer in the discordant width case (ω=0.75); b. (right) Vertical profiles of the dimensionless (with respect to 10^6 x U_d^2) Reynolds shear stress ($\overline{u'v'}$) in the core of the mixing layer in the discordant width case (ω=0.75).

Water surface elevations

In order to assess the influence of the width discordance onto the water surface elevations, the curved rigid-lids (Figure 2) of the discordant and concordant width cases can be compared. It is obvious that the backwater effect is lower in the discordant width case, because of the wider downstream channel. Similarly, the water surface dip in the flow contraction (and recirculation) zone, is less pronounced in the discordant width case.

Mean flow

Based on the time-averaged flow fields, the RZ dimensions (i.e. the maximum width $W_{RZ,\,max}$ and the length L_{RZ}, see Figure 1) are determined by applying the *isovel method* (see e.g. Qing-Yuan et al., 2009; Schindfessel et al., 2015). This means that the RZ boundaries are retrieved from the calculated contourline corresponding to a zero longitudinal velocity component, where its maximum excursion from the downstream channel's inner bank determines $W_{RZ,max}$, while its downstream intersection with the aforementioned bank determines L_{RZ}. Table 4 summarizes the time-averaged dimensions of the RZ in three horizontal planes, with different elevations above the bed, for both the discordant width and the concordant width cases. Note that the predicted near surface (i.e. at z/h_d=0.80) value of $W_{RZ,max}$= 0.27W_d for the discordant width case is slightly larger than the experimental value of $W_{RZ,max}$= 0.23W_d at the water surface (see Fig. 3b in Yuan et al., 2016).

Table 4. RZ dimensions (see Figure 1).

	ω=1.00 (W_d=0.30m; h_d=0.197m)		**ω=0.75 (W_d=0.40m; h_d=0.163m)**	
Location	L_{RZ}	$W_{RZ,max}$	L_{RZ}	$W_{RZ,max}$
z/h_d=0.12	2.50W_d	0.23W_d	1.52W_d	0.13W_d

https://doi.org/10.26077/z99p-xs05

z/h_d=0.50	$2.49W_d$	$0.24W_d$	$1.76W_d$	$0.27W_d$
z/h_d=0.80	$2.48W_d$	$0.24W_d$	$1.84W_d$	$0.27W_d$

As was already deduced by observation of Figure 3, the RZ dimensions in the discordant width case seem to be substantially smaller near the bed as compared to higher in the water column. Moreover, the near bed value of $W_{RZ,max}$ may even be somewhat smaller than predicted (see section 4.1), which means that the 3D effects in the RZ shape are even more pronounced than the simulations suggest. For the concordant width case, however, Table 4 shows that the simulated RZ dimensions do not change significantly over the flow depth.

As can be seen from the vertical sections near the inner bank of the downstream channel (Figure 5), the differences between the RZ dimensions of the discordant and concordant width cases are related to differences in flow structure. More specifically, a pronounced upwelling flow occurs in the discordant width case (around $x/W_d \approx 1.3$) which results near the bed in a longitudinal extent of the RZ that does not start at the downstream confluence corner. In other words: the total length of the RZ is smaller than the $L_{RZ}=1.52W_d$ value indicated in Table 4 (which represents the distance from the downstream corner to the point where the u=0 isoline reattaches to the wall).

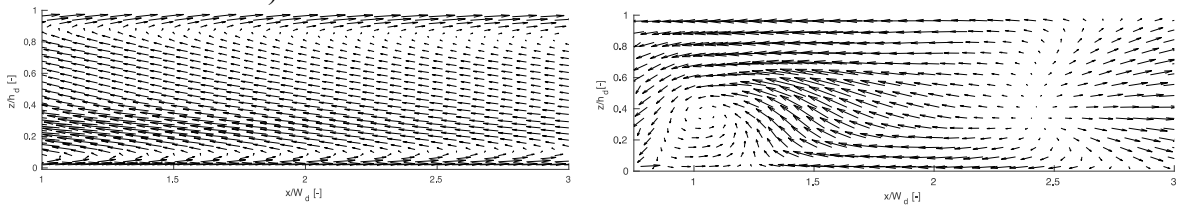

Figure 5. Time-averaged velocity vectors (*u,w*) in a vertical section near the inner bank of the downstream channel (left: section at y/W_d=0.0375 for ω=1.00 case, right: section at y/W_d=-0.2125 for ω=0.75 case).

The top panels of Figure 6 show mean flow streamlines originating from locations at an elevation of z/h_d=0.12 in the upstream main channel. It is clear that the flow contraction is lower in the discordant width case. Similarly, the bottom panels of Figure 6 show mean flow streamlines originating from locations at an elevation of z/h_d=0.12 in the tributary channel, revealing complex flow behaviour. By means of similar streamline plots originating at different elevations above the bed (not shown) it was found that hardly any fluid from the upstream main channel enters the recirculation zone.

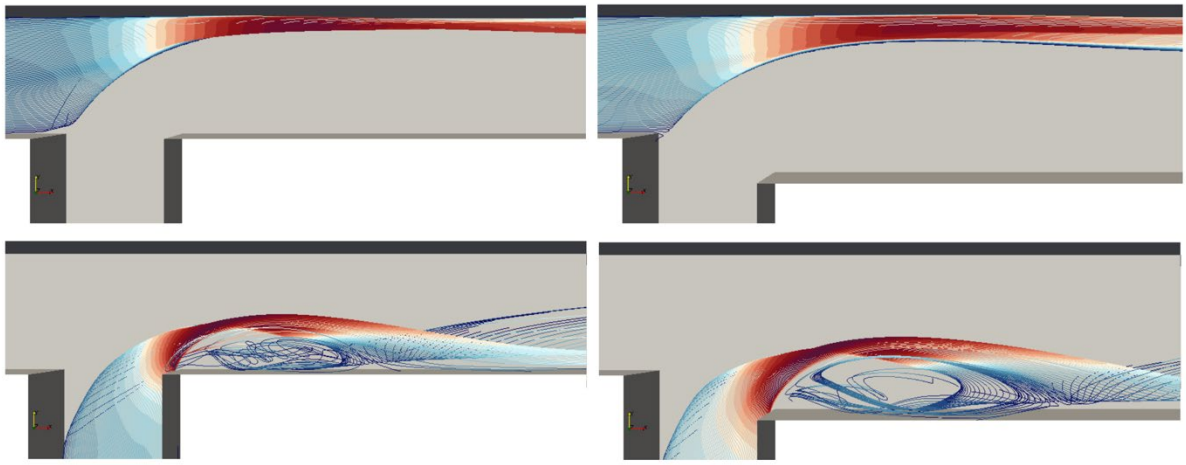

Figure 6. Streamlines of mean flow. Left panels: concordant width case (ω=0.75), right panels: discordant width case (ω=0.75). Top panels: streamlines originating from upstream main channel at an elevation of z/h_d=0.12. Bottom panels: streamlines originating from tributary channel at an elevation of z/h_d=0.12.

Turbulent flow

In Figure 7a, the cross-sectional distribution of the dimensionless TKE and dimensionless Reynolds shear stress ($\overline{u'v'}$), respectively, is presented in three different cross-sections. In every cross-section, a core of higher values persists over the flow depth. Note that the lateral position of those TKE and $\overline{u'v'}$ cores do not coincide.

The concordant width case shows higher values of the dimensionless TKE and $\overline{u'v'}$ (Figure 7b) of the abovementioned cores. The results also show a more pronounced distortion of those cores over the water depth, in the discordant width case. This happens already quite upstream ($1/4<x/W_d<1$). This higher degree of tilting may be linked to the reduced dimensions of the mean flow recirculation zone (RZ) in the near bed zone.

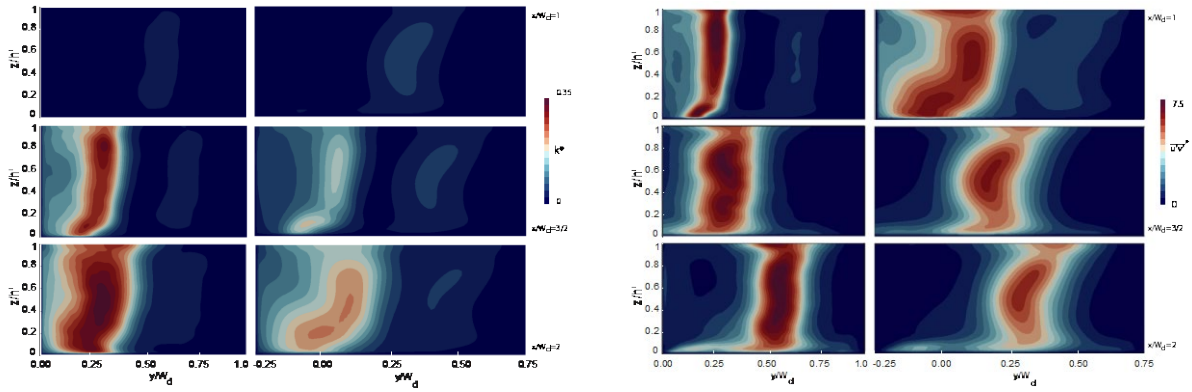

Figure 7. a. (left) Cross-sectional distribution of dimensionless TKE ($k^*=TKE/U_d^2$) for the concordant (ω=1.00, left) and discordant (ω=0.75, right) width cases in three cross-sections (x/W_d=1;3/2;2) of the downstream channel; b. (right) Cross-sectional distribution of dimensionless (with respect to 10^6 x U_d^2) Reynolds shear stress ($\overline{u'v'}$) for the concordant (ω=1.00, left) and discordant (ω=0.75, right) width cases in three cross-sections (x/W_d=1/2;3/2;2) of the downstream channel.

DISCUSSION AND CONCLUSIONS

The effects onto the confluence hydrodynamics of a discordance between the width of the downstream channel and the width of the confluent channels were investigated numerically, for one flow situation (i.e. one flow ratio q and downstream Froude number Fr_d). The widening of the downstream channel was shown to reduce the backwater effects, the flow contraction and the associated water surface depression. Moreover, the width and length of the RZ in the lowest third of the water column were reduced. This seems to be related to a complex mean flow field, including important upwelling motions. To some extent, the foregoing observations are comparable to what was found in confluences with discordant bed elevation, in which the tributary is shallower than the main channel (Biron et al., 1996; Ramos et al., 2019b). In the latter case, however, the RZ was found to be fed by mean flow coming from both the tributary and the upstream main channel (Best and Roy, 1991; Ramos et al., 2019b), whereas in the present case, only the tributary mean flow contributes. With respect to the dimensionless TKE and Reynolds shear stress, the widening of the downstream channel was shown to reduce the peak values in the respective cores of these turbulent quantities. Moreover, the shape of those cores was found to be more distorted, especially in the near bed zone. In future research, it is worth investigating whether the aforementioned observations induce a distortion of the mixing layer between the merging flows, as suggested by Biron et al. (1996) in the context of discordant bed confluences. In addition to this, the possible intermittent and/or periodic character of the flow features discerned in the time-averaged flow (Bradbrook et al., 2000; Parsons, 2003; Yoshimura et al., 2016) should be studied. Finally, the dependency of the effects of width discordance on the flow ratio needs to be investigated. To this end, the developed numerical model for the discordant width flume of Yuan et al. (2016) will be further validated at different flow ratios, based on the experimental data reported in Yuan et al. (2016) and Tang et al. (2018).

ACKNOWLEDGEMENTS

This work was performed using the computational facilities of the HPC infrastructure of Ghent University.

REFERENCES

Best, J. L. and Roy, A. G. (1991). Mixing-layer distortion at the confluence of channels of different depth. Nature, 350(6317), 411. doi.org/10.1038/350411a0.

Best, J.L. (1987). Flow dynamics at river channel confluences: implications for sediment transport and bed morphology. In: Ethridge, F.G. Flores, R.M. Harvey, M.D. (Eds.), Recent developments in

fluvial sedimentology. Spec. Publ. Soc. Sediment. Geol. SEPM 39, 27-35. doi.org/10.2110/pec.87.39.0027.

Birjukova-Canelas, O., Ferreira, R. M., Guillén-Ludeña, S., Alegria, F. C. and Cardoso, A. H. (2019). Three-dimensional flow structure at fixed 70° open-channel confluence with bed discordance. Journal of Hydraulic Research, 1-13. doi.org/10.1080/00221686.2019.1596988

Biron, P., Best, J.L. and Roy, A.G. (1996). Effects of bed discordance on flow dynamics at open channel confluences. Journal of Hydraulic Engineering, ASCE, Vol. 122(12), 676-682. doi.org/10.1061/(ASCE)0733-9429(1996)122:12(676).

Boyer, C., Roy, A. G. and Best, J. L. (2006) Dynamics of a river channel confluence with discordant beds: Flow turbulence, bed load sediment transport and bed morphology. Journal of Geophysical Research: Earth Surface, 111(F4). doi.org/10.1029/2005JF000458.

Bradbrook, K.F., Lane, S.N., Richards, K.S., Biron, P.M. and Roy, A.G. (2000). Large Eddy Simulation of periodic flow characteristics at river channel confluences. Journal of Hydraulic Research, 38(3), 207-215. doi.org/10.1080/00221680009498338.

Constantinescu, G., Miyawaki, S., Rhoads, B., Sukhodolov, A. and Kirkil, G. (2011). Structure of turbulent flow at a river confluence with momentum and velocity ratios close to 1: Insight provided by an eddy-resolving numerical simulation. Water Resources Research, 47(5).

Cushman-Roisin, B. and Constantinescu, G.S. (2019). Dynamical adjustment of two streams past their confluence. Journal of Hydraulic Research, 1-9. doi.org/full/10.1080/00221686.2019.1573765.

De Serres, B., Roy, A. G., Biron, P. M. and Best, J. (1999) Three-dimensional structure of flow at a confluence of river channels with discordant beds. Geomorphology, 26(4), 313-335. doi.org/10.1016/S0169-555X(98)00064-6.

Đorđević, D. (2013) Numerical study of 3D flow at right-angled confluences with and without upstream planform curvature. Journal of Hydroinformatics, 15(4), 1073-1088. doi.org/10.2166/hydro.2012.150.

Yoshimura, H., Fujita, I., Ichiro Moriguchi, R. (2016) Numerical and experimental investigations of unsteady separation zone generated at a right-angled confluence. RiverFlow16, doi.org/10.1201/9781315644479-251.

Huang, J., Weber, L.J. and Lai, Y.G. (2002) Three-dimensional numerical study of flows in open-channel junctions. Journal of Hydraulic Engineering, 128(3), 268-280.

Parsons, D. R. (2003). Discussion of "Three-dimensional numerical study of flows in open-channel junctions" by Jianchun Huang, Larry J. Weber, and Yong G. Lai. Journal of Hydraulic Engineering, 129(10), 822-823.

Penna, N., De Marchis, M., Canelas, O. B., Napoli, E., Cardoso, A. H. and Gaudio, R. (2018) Effect of the junction angle on turbulent flow at a hydraulic confluence. Water 10(4), 469-491.

Qing-Yuan, Y., Xian-Ye, W., Wei-Zhen, L., & Xie-Kang, W. (2009). Experimental study on characteristics of separation zone in confluence zones in rivers. Journal of Hydrologic Engineering, 14(2), 166-171.

Rameshwaran, P. and Naden, P. S. (2004) Three-dimensional modelling of free-surface variation in a meandering channel. Journal of Hydraulic Research, 42, 603–615.

Ramos, P.X., Schindfessel, L., Pêgo, J.P. and De Mulder, T. (2019a) Flat vs. curved rigid-lid LES computations of an open-channel confluence. Journal of Hydroinformatics, 21, no.2: 318-334. doi.org/10.2166/hydro.2019.109

Ramos, P.X., Schindfessel, L., Pêgo, J.P. and De Mulder, T. (2019b) Rigid-lid LES predictions of secondary ow in an open-channel confluence with concordant and discordant beds. 38th IAHR World Congress, Panama.

Rice, S., Roy, A., & Rhoads, B. (2008). River confluences, tributaries and the fluvial network. John Wiley & Sons.

Rodi, W., Constantinescu, G. and Stoesser, T. (2013). Large-eddy simulation in hydraulics. CRC Press.

Schindfessel, L., Creëlle, S. and De Mulder, T. (2015). Flow patterns in an open channel confluence with increasingly dominant tributary inflow. Water, 7(9), 4724-4751. doi.org/10.3390/w7094724.

Tang, H., Zhang, H. and Yuan, S. (2018). Hydrodynamics and contaminant transport on a degraded bed at a 90-degree channel confluence. Environmental Fluid Mechanics, 18(5), 1293-1295. http://dx.doi.org/10.1007/s10652-018-9612-x

Talebpour, M. and Liu, X., 2019. Numerical investigation on the suitability of a fourth-order nonlinear k-ω model for secondary current of second type in open-channels. Journal of Hydraulic Research, 57(1), pp.1-12.

Weber, L. J., Schumate, E. D. and Mawer, N. (2001) Experiments on flow at a 90° open-channel junction. Journal of Hydraulic Engineering, 127(5), 340-350. doi.org/10.1061/(ASCE)0733-9429(2001)127:5(340).

Winant, C. D., and Browand, F. K. (1974). "Vortex pairing: The mechanism of turbulent mixing layer growth at moderate Reynolds number," Journal of Fluid Mechanics, 63, 237-255.

Yang, Q. Y., Liu, T. H., Lu, W. Z. and Wang, X. K. (2013) Numerical simulation of confluence flow in open channel with dynamic meshes techniques. Adv. Mech. Eng., 5, 860431.

Yuan, S., Tang, H., Xiao, Y., Qiu, X., Zhang, H. and Yu, D. (2016) Turbulent flow structure at a 90-degree open channel confluence: accounting for the distortion of the shear layer. Journal of Hydroenvironmental Research, 12, 130-147.